ACS APPLIED MATERIALS & INTERFACES

Research Article

www.acsami.org

One-Step Carbonization Synthesis of Hollow Carbon Nanococoons with Multimodal Pores and Their Enhanced Electrochemical Performance for Supercapacitors

Jianan Zhang,[†] Kaixi Wang,[†] Shaojun Guo,*[,‡] Shoupei Wang,[†] Zhiqiang Liang,[§] Zhimin Chen,[†] Jianwei Fu,[†] and Qun Xu*[,†]

[†]College of Materials Science and Engineering, Zhengzhou University, Zhengzhou 450052, People's Republic of China

[‡]Physical Chemistry and Applied Spectroscopy, Los Alamos National Laboratory, Los Alamos, New Mexico 87545, United States

[§]State Key Laboratory of Inorganic Synthesis and Preparative Chemistry, College of Chemistry, Jilin University, Changchun 130012, People's Republic of China

Supporting Information

ABSTRACT: Hollow carbon capsules with multimodal pores are highly promising for developing novel electrode materials for high-performance electrochemical devices due to their more active sites for ion and electron transfer. However, at present, most of the previous efforts are focused on the multistep process for the synthesis of hollow carbon nanostructures with individual pores. Herein, hollow carbon nanococoons (HCNCs) with non-spherical cavity and multimodal hierarchical pores have been facilely synthesized via a one-step carbonization of a Fe_2O_3/carbon precursor core/shell nanospindle at 850 °C. We interestingly found that during the carbonization, Fe_2O_3 was automatically "escaped" from the inside nanospindle, leading to the formation of new HCNCs. Most importantly, the spindle-shaped cavity of the obtained HCNCs with high conductivity can offer a multimodal ion diffusion pathway, which can facilitate the reaction kinetics in a supercapacitor. As a result, the HCNCs-based supacapacitor exhibits the capacitance of 220.0 F g^{-1} at a given scan rate of 5 mV s^{-1}, 3.5 times higher than that of hollow carbon spheres, high stability with 98% of the initial capacity maintained even after 1000 cycles, and high rate capability. This work provides a new and facile avenue for enhancing performance of a HCNCs-based supercapacitor by using the non-spherical hollow structures with multimodal pores.

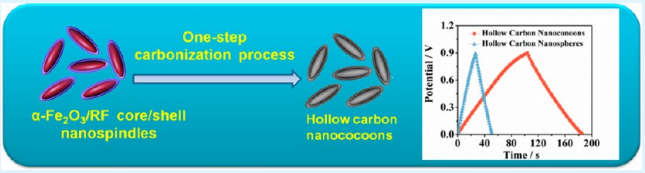

KEYWORDS: *hollow carbon capsules, one-step carbonization, hollow carbon nanococoon, microporous materials, supercapacitor*

1. INTRODUCTION

Synthesis of hollow carbon spheres (HCSs) has received a great deal of interest owing to their merits of low density and large surface area as well as for their important technological applications in gas storage, catalysis, battery and electronic devices.[1−7] Among the numerous strategies for preparing HCSs, the hard template approach is the most effective one, which provides nice opportunities for various porous carbon nanostructures. Typical examples include the synthesis of HCSs with silica[8−10] or polystyrene particles as a template,[11,12] and making carbon nanocages using MgO[13] and MnO particle as a template,[14,15] etc. Recent studies reveal that hollow non-spherical capsules (HNSCs) are of even more interest because of their distinct advantages in longitudinal ion and electron transfer for energy conversion and storage.[16−19] For instance, Archer and co-workers prepared hollow TiO_2 nanococoons by a surfactant assistant template method, which showed enhanced lithium storage capability compared to TiO_2 solid microspheres.[17] Wang et al. found that hollow α-Fe_2O_3 nanococoons, prepared by phase transition under high temperature, exhibited a better photocatalytic performance than the commercial α-Fe_2O_3 nanoparticles (NPs).[19] Although these HNSCs show the obvious advantages in electrochemical and photoelectrochemical performance, their synthesis requires a multistep complex process, which is usually conducted by coating the surface of a colloidal particle template with a layer of desired materials, followed by the selective removal of the colloidal template through wet chemical etching. Such a process can not only introduce the risk for damaging the hollow structure by additionally removing the core template but also bring some uncertain in estimating the property of HCSs due to the potential insufficient removal of core materials. Therefore, exploring one-step routes for the preparation of HNSCs is greatly needed and has become a challenging topic.

As a promising future energy storage device, supercapacitors have attracted more considerable interest for their unique advantages of high power density, long lifespan, and a good charge−discharge characteristic. HCSs have been widely

Received: November 26, 2013
Accepted: January 16, 2014
Published: January 16, 2014

   dx.doi.org/10.1021/am405375s | ACS Appl. Mater. Interfaces 2014, 6, 2192−2198

studied as a vital candidate for an electron double layer capacitor (EDLC) because of their high surface area and high conductivity. Various groups have focused on the design of advanced HCSs with well-organized pore structures for promoting the performance of supercapacitors.[20−22] These have been well-demonstrated in the controlled synthesis of hollow carbon capsules with specific capacitance from 95 to 122 F g^{-1},[20] hollow carbon capsules by the use of thioether-drived bridged organosilica with the specific capacitance of 80 F g^{-1},[21] and porous carbon hemispheres with specific capacitance of 83 F g^{-1}, etc.[22] Despite their great potentials in supercapacitor applications, these existing studies lack in pore tunability and multimodality, which is hard to maximize the surface area of carbon nanomaterials, and thus results in relatively low performance. In searching for more robust and practical electrode materials for higher performance supercapacitors, the development of hollow-structured carbon with multimodal pores spanning from micropore, mesopore to macropore, and also a 3D large internected channel network is highly desirable. Such a structure will be very important for maximizing both electron and ion transfer, thus allowing for efficient charge and mass exchange that occurs when charging/discharging a capacitor.

In this article, we demonstrate a simple, cost-effective, and environmental friendly synthetic strategy for the synthesis of HCNCs with multimodal pores of 0.8, 1.82, 4.25, 6.43 nm and 100 nm (cavity), indicating the coexistence of a hierarchical micropore, mesopore, and macropore in HCNCs. Such a particular nanostructure is highly important for enhancing supercapacitor application. Our results reveal that HCNCs exhibit the capacitance of 220.0 F g^{-1}, which is 3.5 times higher than that of HCSs. And also, they are stable for a supercapacitor with 98% of the initial capacity maintained even after 1000 cycles. We expect that such HCNCs with multimodal pores will also be important for developing other energy devices such as fuel cells and lithium batteries.

2. EXPERIMENTAL SECTION

2.1. Materials. Iron(III) chloride anhydrous, sodium dihydrogen phosphate dihydrate, and ethanol were purchased from Sinopharm Chemical Reagent Co., Ltd. Resorcinol, formaldehyde, and ammonium hydroxide were obtained from the Tianjin Chemical Factory. All chemicals were used as received without any further purification. Deionized water was used in all experiments.

2.2. Synthesis of Hollow Carbon Nanococoons. The spindle-like α-Fe_2O_3 particles were prepared by aging a solution of 0.02 M $FeCl_3$ and NaH_2PO_4 at 105 °C for 48 h.[23,24] For a typical coating of RF resin, 14.4 mg of α-Fe_2O_3 particles was first dispersed by utrasonication in a mixture consisting of 2 mL of ethanol and 2 mL of deionized water, followed by 10 μL of ammonia (28%). After ultrasonication for 10 min, 10 mg of resorcinol and 14 μL of formaldehyde were sequentially added into the above solution. The resulting mixture was sonicated for 30 min and transferred to a Teflon-lined stainless-steel autoclave and heated at 100 °C for 24 h. The obtained solid was harvested by centrifugation, washed with water and ethanol, followed by drying at 50 °C overnight. Then, the as-prepared α-Fe_2O_3@RF core/shell nanospindles were annealed at 850 °C for 4 h with a heating rate of 1 °C/min under N_2 atmosphere. Subsequently, the carbonized product was ultrasonically dispersed in 20 mL of ethanol. After aging for 2 h, the hollow carbon nanococoons were obtained from the upper black "ink" by centrifugation and drying.

2.3. Synthesis of Hollow Carbon Spheres. 1.25 mL of ammonia solution (32 wt %) was added to 40 mL of ethanol/water mixture (ethanol/water volume ratio = 2). The solution was stirred at 30 °C for 30 min, followed by the dropwise addition of 1.4 mL of tetraethyl orthosilicate under vigorous stirring, 0.2 g of resorcinol after 30 min, and 0.28 mL of formaldehyde solution after another 10 min. The mixture was stirred for 24 h at 30 °C, then transferred to a Teflon-lined stainless-steel autoclave and heated at 100 °C for 24 h. The resulted solid was harvested by centrifugation, washed with water and ethanol, followed by drying at 50 °C overnight. Then, as-prepared silica/RF core/shell particles were annealed at 850 °C for 1 h with a heating rate of 5 °C/min under N_2 atmosphere. Subsequently, the carbonized product (silica/carbon spheres) was treated with hydrofluoric acid (15 wt %) to dissolve the silica core.

2.4. Characterizations. Transmission electron microscopy (TEM) images were collected on a Tecnai G2 20 with an accelerating voltage of 200 KV. Scanning electron microscopy (SEM) images were taken by a field-emission scanning electron microscope (JEOL 7500) operating at 5 KV. The X-ray diffraction (XRD) pattern of the product was recorded on a Rigaku D/MAX-3B using Cu Kα radiation (λ = 1.5406 Å). The thermal decomposition behavior of the samples was monitored using a Mettler Toledo TGA/DSC 1 analyzer from 30 to 900 °C under air with a heating rate of 10°C/min. The nitrogen sorption experiment was carried out at 77 K on a Micromeritics Tristar 2200 system with micropore analysis. The Brunauer−Emmett−Teller (BET) specific surface area was calculated using adsorption data at a relative pressure range of P/P_0 = 0.05−0.25. The pore volumes were estimated from the amounts adsorbed at a relative pressure (P/P_0) of 0.99. The electrochemical impedance spectroscopy (EIS) was measured in the frequency range of 10 mHz to 10 kHz at the open circuit voltage with an alternate current amplitude of 5 mV.

2.5. Electrochemical Measurements. The capacitance performances of the sample were evaluated in the two-electrode system at ambient conditions. The sample was prepared onto a thin film according to the protocol described in a previous study.[13] Simply, the active material suspension with a concentration of 2.0 mg $mL^{-1}$was prepared by sonicating 2 mg of active materials in a 1 mL of ethanol containing Nafion (Dupont, 5 wt %) at a volume ratio of 9.6:0.4. Then, 25 μL of ink was dropped onto the glassy carbon disk with a diameter of 5 mm and dried thoroughly in air. The electrochemical measurements were carried out in 1 M KOH solution. Two symmetry electrodes with a distance of 15 mm between the centers were immersed into a beaker containing 1 M KOH solution. The capacitances C_s (F g^{-1}) based on the CVs were calculated by

$$C_s = \frac{\int I d\varphi}{V \times E \times m} \quad (1)$$

where I is the current (A), φ is the potential (V), $\int I d\varphi$ is the area of the CV loop, V is the potential scan rate (V s^{-1}), and m is the effective mass of the active electrode materials (g). The capacitances C_m (F g^{-1}) based on the discharge curves were calculated by

$$C_m = 4 \times \frac{I \times \Delta t}{U \times m} \quad (2)$$

where I is the discharge current (A), Δt are the discharge times (s), U is the voltage range (V), and m is the total mass of the active materials on both electrodes.

3. RESULTS AND DISCUSSION

HCNCs with a spindle-like inner cavity (20 nm in width and 100 nm in length) and hierarchical pores (0.8, 1.82, 4.25, 6.43 nm) were facilely prepared through a one-step carbonization process (Scheme 1). Briefly, (a) the spindle-like α-Fe_2O_3 NPs were first synthesized according a reported procedure,[23,24] and further directly and uniformly coated with resorcinol−formaldehyde (RF) resin in an ethanol−water−ammonia system. (b) The obtained powder was carbonized at a high temperature (850 °C) under N_2 atmosphere, which simultaneously allowed the "escape" of α-Fe_2O_3 core from the carbon shell. Our synthetic process is simpler, which is different from the previous template approach that involves coating a carbon

Scheme 1. Schematic Process for the Preparation of HCNCs

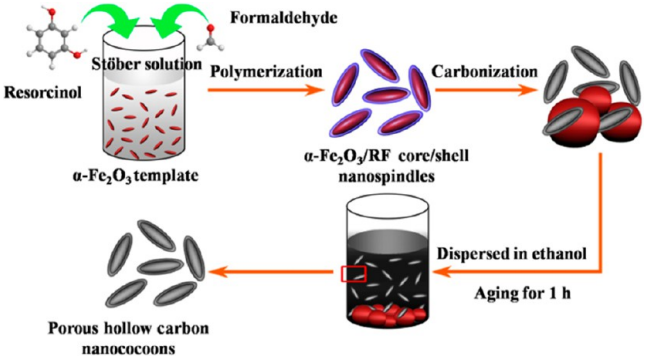

precursor on a hard template core, followed by carbonization and an additional core removal process. To the best of our knowledge, this is the first report on the use of a one-step carbonization process in order to remove the core template and, in the meantime, achieve hollow carbon capsules.[25] HCSs were also synthesized through the use of SiO_2 nanospheres as template instead of spindle-like α-Fe_2O_3 NPs. Simply, the SiO_2 nanospheres (250 nm in diameter) were first coated with the RF resin via the Stöber method,[26,27] followed by carbonization and the removal of the SiO_2 template with hydrofluoric acid. The scanning electron microscopy (SEM) and transmission electron microscopy (TEM) images of HCSs are shown in Figure S1 (Supporting Information). These hollow HCSs with a diameter of about 270−280 nm and a cavity size of about 200 nm were used as a control to demonstrate the distinct electrochemical performance of HCNCs.

Figure 1a,b shows the typical SEM (Figure 1a) and TEM (Figure 1b) images of the as-synthesized α-Fe_2O_3 nanospindles. They have an average length of 180 nm and width of 40 nm. The magnified TEM image (Figure 1b) reveals that α-Fe_2O_3 nanospindles possess a rough structures consisting of tiny crystals. Figure 1c,d gives the TEM images of α-Fe_2O_3/RF core/shell nanospindles at different magnifications. It is found that all α-Fe_2O_3 nanospindles are uniformly coated by a thin RF resin layer with a thickness of about 10 nm, indicating the efficiency of our method. X-ray diffraction (XRD) patterns of α-Fe_2O_3 spindles and α-Fe_2O_3/RF core/shell nanospindles are shown in Figure S2a (Supporting Information), matching well with the diffraction peaks of α-Fe_2O_3 powder (standard JCPDS, No. 86-0550). This confirms the presence of the crystalline α-Fe_2O_3 after coating with RF resin. Figure 1e,f depicts the TEM images of the as-prepared HCNCs at different magnifications. All HCNCs with an average shell thickness of about 8 nm keep a hollow spindle-like morphology, and no α-Fe_2O_3 residues were observed in the cavities. High-resolution TEM (HRTEM) image (Figure 2a), XRD pattern (Figure 2b) and Raman spectroscopy (Figure 2c) of HCNCs were further used to reveal the carbon phases and the crystallinity of carbon shell. Their HRTEM image illustrates that the small crystalline regions are formed by 3−10 parallel fringes with an interlayer *d*-spacing of 0.375 nm. The XRD pattern of the HCNCs show two diffraction peaks centered at 25.4 °C and 43.7 °C, corresponding to the (101) and (002) diffractions from the graphitic phase, respectively, further indicating that HCNCs have good crystallinity. Furthermore, Raman spectrum of HCNCs show the higher ratio of I_G/I_D (I_D and I_G are related to the A_{1g} vibration mode of the disordered carbon (D-bond) and the E_{2g} vibration mode of the ordered graphitic carbon (G-bond)) than that of reduced graphene oxide.[28−30] These proofs from HRTEM, XRD, and Raman spectroscopy reveal that the carbon shell features graphitic order with small crystalline domains, promising good conductivity. In addition, thermogravimetric analysis (TGA) of HCNCs (Figure S2b, Supporting Information) shows that no remaining exists in the product after 850 °C. Thus, both the TEM and TGA results prove that the α-Fe_2O_3 template was effectively removed from the α-Fe_2O_3/RF core/shell nanospindles during carbonization.

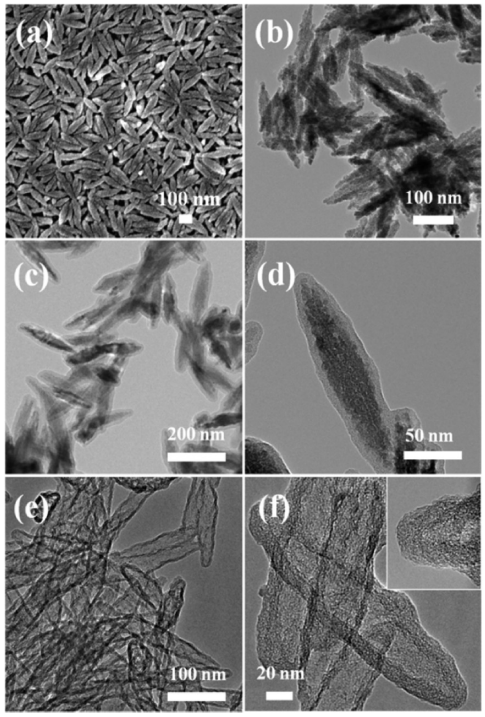

Figure 1. Representative SEM (a) and TEM (b) images of α-Fe_2O_3 nanospindles. TEM images of α-Fe_2O_3/RF core/shell nano spindles (c, d) and HCNCs (e, f) at different magnification. Inset of panel f shows the detailed structure of the corresponding samples at high magnification.

To investigate the removal process of the α-Fe_2O_3 template during carbonization, the morphological changes of the composite nanospindles (noted as Fe−C samples) at different carbonization temperatures were monitored by TEM technique (Figure 3). An interesting phenomenon occurred with the increase of temperature. The nanospindle cores first disintegrated into smaller particles at 450 °C (Figure 3a). When the carbonization temperature increased to high temperatures such as 650 and 850 °C, the nanospindles template gradually disappeared and fused into big particles outside the HCNCs (Figure 3b,c). These big particles were easily precipitated from the solution, making us get HCNCs with high yield (Figure 3d). The crystalline structure changes of the composite nanospindles at different carbonization temperature were also investigated, as shown in the XRD patterns of Figure 4. We found that the intensity of the diffraction peaks of the Fe-containing species varies with the carbonization temperatures. Ion species (bcc-Fe) and Fe_3O_4 are presented in the Fe−C samples carbonized at 450 °C, whereas for the Fe−C samples carbonized at 650 °C, partial Fe-containing species converted to the Fe_3C species.[31−33] As the temperature further increased to 850 °C, the diffraction peak of Fe_3C becomes stronger, indicating the increase of the fused ion−carbon phase. The

dx.doi.org/10.1021/am405375s | ACS Appl. Mater. Interfaces 2014, 6, 2192−2198

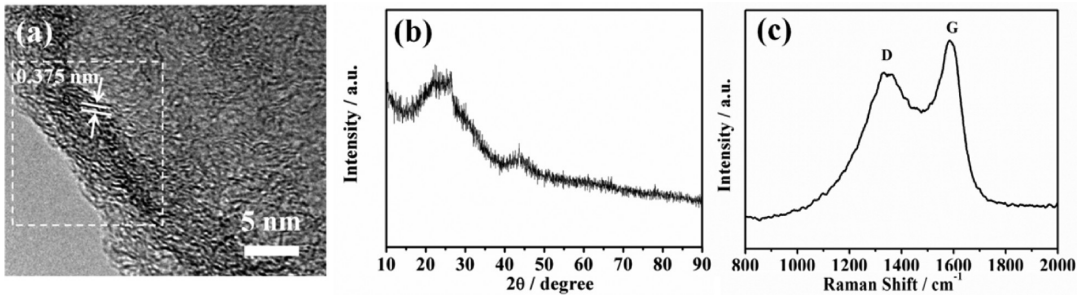

Figure 2. (a) HRTEM image, (b) X-ray diffraction pattern, and (c) Raman spectrum of HCNCs.

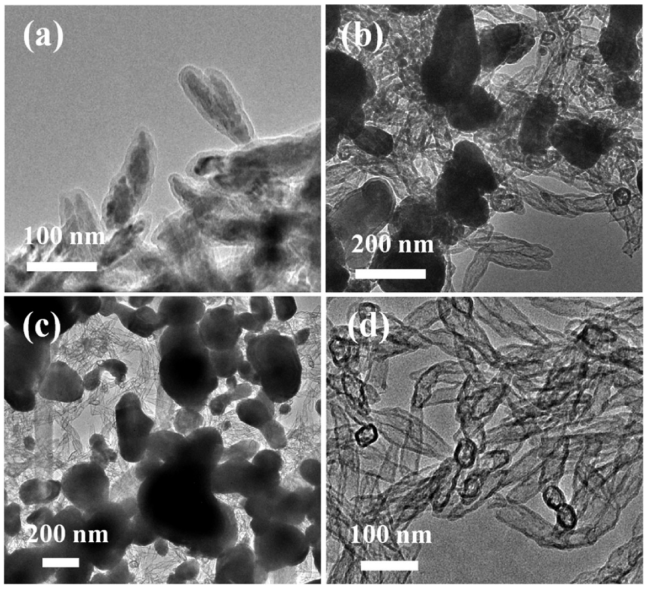

Figure 3. Investigation of the α-Fe_2O_3 removal process during carbonization. TEM images of α-Fe_2O_3/RF core/shell nanospindles carbonized at different temperature: (a) 450 °C, (b) 650 °C, and (c) 850 °C. (d) HCNCs obtained from sample (c).

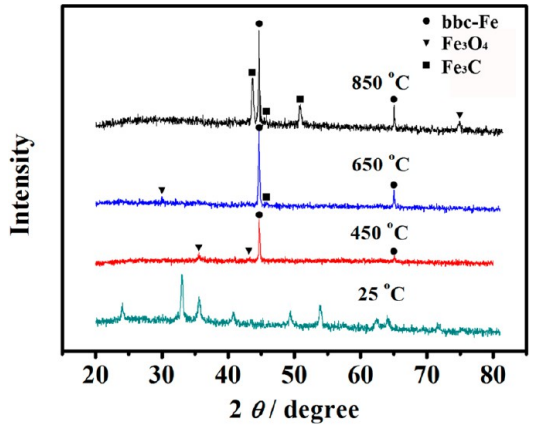

Figure 4. XRD patterns of as-prepared α-Fe_2O_3/RF core/shell nanospindles at room temperature and carbonized at different temperature: 450, 650, and 850 °C.

XRD results demonstrate that the Fe_2O_3 particle cores are reduced by carbon with increases to the carbonization temperature. On the basis of the above evidences, we suppose that the formation of hollow structured HCNCs is probably related to the temperature-induced nanosized Fe-containing species diffusion and fusion process.[34]

The N_2 adsorption−desorption isotherms and pore distribution of the HCNCs are shown in Figure 5. The isotherm exhibits combined characteristics of type I and IV with a well-defined knee at the low P/P_0 (0−0.1) and clear hysteresis loops (Figure 5a). The H3-type hysteresis loop at P/P_0 between 0.8 and 1.0 is attributed to the inner hollow cavity of HCNCs.[3] HCNCs have a BET surface area of 390 $m^2\ g^{-1}$, a micropore surface area of 153 $m^2\ g^{-1}$ (the t-plot method), and a total pore volume of 0.65 $cm^3\ g^{-1}$.[35−37] The pore size distribution (PSD) for adsorption data, based on the Barrett−Joyner−Halenda (BJH) method is given in Figure 5b. The HCSSs have sharp peaks at 0.8, 1.82, 4.25, and 6.43 nm, indicating the coexistence of hierarchical micropores, mesopores, and macropores (cavity of HCNCs) in the sample, in good agreement with the observation results obtained by TEM (Figure 1e,f). All this evidence indicates that the HCNCs have a hierarchical porous structure with a micro/mesopore shell and a macropore cavity.

To evaluate the electrochemical properties of the HCNCs-based supercapacitor, cyclic voltammetry (CV) and galvanostatic charge−discharge measurements were carried out with a two-electrode system in 1.0 M KOH.[13,38] Simply, the active materials were redispersed in ethanol containing Nafion (5 wt %) to reach a concentration of 2 mg mL^{-1}. Then 25 μL of this dispersion was deposited on the glassy carbon disk with a diameter of 5 mm. Two symmetry electrodes with a distance of 15 mm between the centers were immersed into a beaker containing 1 M KOH solution (Figure 6). As shown in Figure 6a, CVs of the HCNCs at different scan rates present a rectangular-like shape owing to the effect of electric double-layer capacitance, without a very oblique angle, even at a scan rate as high as 1000 mV s^{-1}. This indicates that HCNCs have a highly capacitive nature and a small equivalent series resistance (ESR) under rapid charging−discharging process.[39−41] Figure 6b shows that even at a high scan rate of 1000 mV s^{-1}, the specific capacitance of HCNCs keeps a 65% retention of that at low scan rate of 5 mV s^{-1}, implying a good rate capability. Rate performance of HCNCs has been further investigated using more amounts of HCNCs (e.g., 2 mg), as shown in Figure S3 (Supporting Information). The HCNCs still exhibit the similar good rate capability for supercapacitors. Chronopotentiometry (CP) of the HCNCs in the potential range of 0−0.9 V is shown in Figure 6c. The nearly linear and relatively good symmetric lines indicate a good capacitive behavior with a good reversible property. The specific capacity decreases only by 13.6% after a current density increase from 1 to 20 A g^{-1}, suggesting the good sustainability of capacitance. No obvious Ohmic drop is observed, even at a high current density of 20 A g^{-1} for HCNCs, again proving their small ESR and good capacitive performance during the rapid charging−discharging process.[42−44] Furthermore, cyclic tests were carried out at a

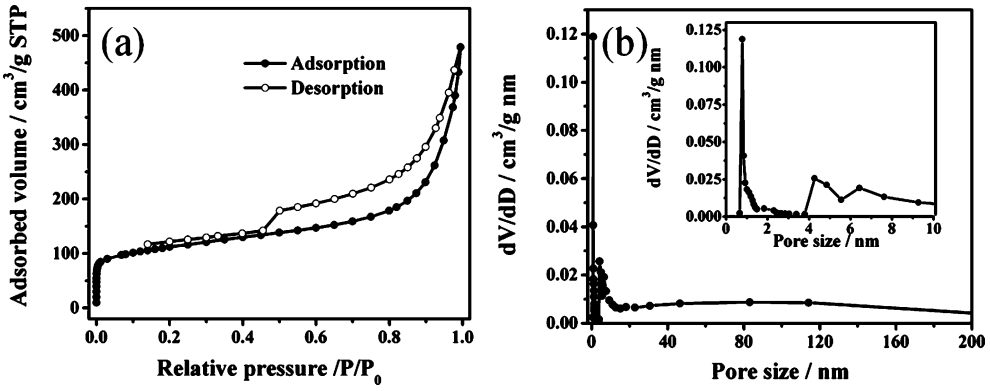

Figure 5. (a) N_2 sorption isotherms and (b) the BJH pore size distribution curves (inset: magnified 0−10 nm region) of HCNCs.

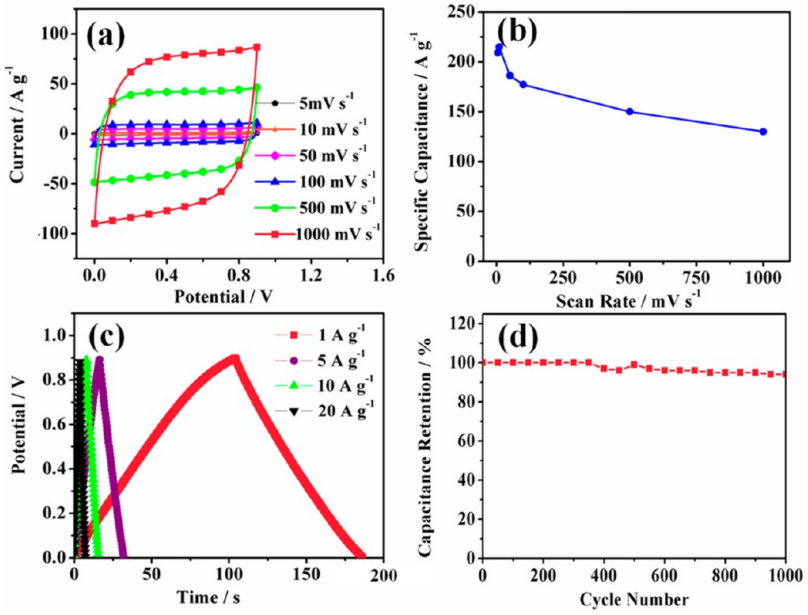

Figure 6. Electrochemical performance of HCNCs electrode with a two-electrode system in 1.0 M KOH. (a) CVs at different scan rates, (b) the corresponding variation of specific capacity with scan rates, (c) galvanostatic charge/discharge curve at different current density, and (d) cycling performance of HCNCs with a current density of 5 A g^{-1}.

constant high charging−discharging current of 5 A g^{-1} (Figure 6d), showing that 98% of the initial capacity can be maintained even after 1000 cycles. Taking into account the high specific capacitance and the excellent electrochemical stability, HCNCs present promise as the electrode candidate for a supercapacitor.

We further compared the capacitance properties of HCNCs with HCSs. Figure 7 gives the CVs and CP of HCNCs and HCSs-based supercapacitors in 1.0 M KOH solution. Significantly, HCNCs show a remarkably better performance than HCSs. At a given scan rate of 5 mA s^{-1}, the specific capacitance of HCNCs is 215.0 F g^{-1} whereas that of HCSs is 62 F g^{-1} (Figure 7a,b). And at a given current density of 1 A g^{-1}, the specific capacitance of HCNCs (183.2 F g^{-1}) calculated from CP is 3.2 times higher than that of HCSs (53.2 F g^{-1}) (Figure 7c,d). It should be noted that HCSs (409.2 m^2 g^{-1}, Figure S4a, Supporting Information) with microporous structures (~0.67 nm, Figure S4d, Supporting Information) shows a relatively larger BET surface area than HCNCs (390.3 m^2 g^{-1}), but much lower capacitance, indicating that the non-spherical cavity coupled with a hierarchical porous structure may play a positive role on enhancing the capacitance. This observation can probably be explained that the non-spherical cavity can serves as a more efficient reactor than the spherical cavity for ion storage and shortening the diffusion length of electrolyte ions.[4] In addition, HCNCs show a lower internal resistance than HCSs, confirmed by the electrochemical impedance data (Figure S5, Supporting Information), further confirming the better electrolyte ions diffusion in the HCNCs-based supercapacitor.

4. CONCLUSIONS

In conclusion, uniform HCNCs with multimodal pores from micropore to mesopore and macropore were simply fabricated by one-step carbonization of α-Fe_2O_3/RF nanospindles. The obtained HCNCs possess excellent structure characteristics including a uniform particle size, hierarchical porous structure, and asymmetric inner cavity. The HCNCs exhibit a maximum specific capacitance of 220 F g^{-1} in KOH electrolyte at 5 mV s^{-1}, which is 3.5 times higher than that of HCSs. They also show excellent cycling stability with 98% of the initial capacity after 1000 cycles. This work also opens new avenue for obtaining other non-spherical hollow capsules that are available for more applications, such as biomedicines, catalysts, photovoltaic cells, and lithium ion batteries.

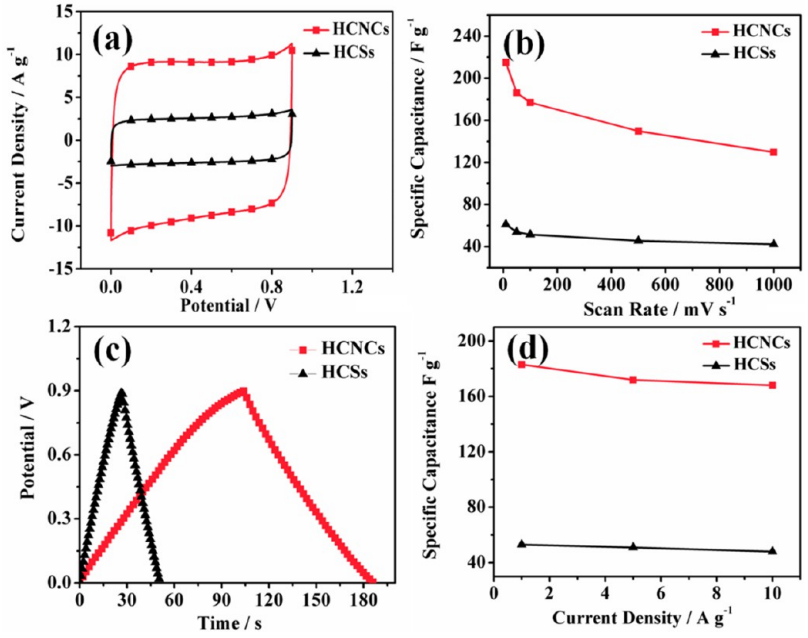

Figure 7. Electrochemical properties of HCNCs and HCSs with a two-electrode system in 1.0 M KOH, respectively. (a) CVs at the scan rate of 100 mV s^{-1}, (b) specific capacitances from CV curves at different scan rates, (c) galvanostatic charge/discharge curves at a current density of 1 A g^{-1}, and (d) specific capacitances calculated from galvanostatic charge/discharge curves versus different current densities.

■ ASSOCIATED CONTENT

Supporting Information

SEM and TEM images of HCNs at different magnifications; XRD patterns of spindle α-Fe_2O_3 and α-Fe_2O_3/RF core/shell nanospindles, respectively; TGA curves of HCNCs and α-Fe_2O_3/RF core/shell nanospindles under air atmosphere with a heating rate of 10 °C min^{-1}, respectively; cyclic voltammograms and specific capacitances (vs scan rate) of HCNCs. This material is available free of charge via the Internet at http://pubs.acs.org.

■ AUTHOR INFORMATION

Corresponding Authors

*Qun Xu. E-mail: qunxu@zzu.edu.cn.

*Shaojun Guo. E-mail: shaojun.guo.nano@gmail.com.

Notes

The authors declare no competing financial interest.

■ ACKNOWLEDGMENTS

This work was financially supported by the National Natural Science Foundation of China (Nos. 21101141 and 51173170), Program for New Century Excellent Talents in Universities (NCET), J. Robert Oppenheimer Distinguished Fellowship and the Open Project Foundation of State Key Laboratory of Inorganic Synthesis and Preparation Chemistry of Jilin University (2012−13).

■ REFERENCES

(1) Lai, X. Y.; Halpert, J. E.; Wang, D. *Energy Environ. Sci.* **2012**, *5*, 5604.

(2) Tang, S. H.; Huang, X. Q.; Chen, X. L.; Zheng, N. F. *Adv. Funct. Mater.* **2010**, *20*, 2442.

(3) Arnal, P. M.; Weidenthaler, C.; Schüth, F. *Chem. Mater.* **2006**, *18*, 2733.

(4) Yang, M.; Ma, J.; Zhang, C. L.; Yang, Z. Z.; Lu, Y. F. *Angew. Chem., Int. Ed.* **2005**, *44*, 6727.

(5) Liu, R.; Mahurin, S. M.; Li, C.; Unocic, R. R.; Idrobo, J. C.; Gao, H. J.; Pennycook, S. J. *Angew. Chem., Int. Ed.* **2011**, *50*, 6799.

(6) Fuertes, A. B.; Valle-Vigón, P.; Sevilla, M. *Chem. Commun.* **2012**, *48*, 6124.

(7) Lu, A. H.; Li, W. C.; Hao, G.; Spliethoff, P. B.; Bongard, H. J.; Schaack, B. B.; Schüth, F. *Angew. Chem., Int. Ed.* **2010**, *49*, 1615.

(8) Bhattacharjya, D.; Kim, M.-S.; Bae, T.-S.; Yu, J.-S. *J. Power Sources* **2013**, *244*, 799.

(9) Han, Y.; Dong, X. T.; Zhang, C.; Liu, S. X. *J. Power Sources* **2012**, *211*, 92.

(10) Yang, Y. J.; Sun, Y. Q.; Su, Q. D. *Chem. Commun.* **2011**, *47*, 12364.

(11) Lu, A.-H.; Sun, T.; Li, W.-C.; Sun, Q.; Han, F.; Liu, D.-H.; Guo, Y. *Angew. Chem., Int. Ed.* **2011**, *50*, 11765.

(12) Fu, J. W.; Xu, Q.; Chen, J. F.; Chen, Z. M.; Huang, X. B.; Tang, X. Z. *Chem. Commun.* **2010**, *46*, 6563.

(13) Xie, K.; Qin, X. T.; Wang, X. Z.; Wang, Y. N.; Tao, H. S.; Wu, Q.; Yang, L. J.; Hu, Z. *Adv. Mater.* **2012**, *24*, 347.

(14) Tan, Y. M.; Xu, C. F.; Chen, G. X.; Liu, Z. H.; Ma, M.; Xie, Q. J.; Zheng, N. F.; Yao, S. Z. *ACS Appl. Mater. Interfaces* **2013**, *5*, 2241.

(15) Tan, Y. M.; Xu, C. F.; Chen, G. X.; Fang, X. L.; Ma, M.; Xie, Q. J.; Zheng, N. F. *Adv. Funct. Mater.* **2012**, *22*, 4584.

(16) Wang, Y.; Su, X. W.; Lu, S. *J. Mater. Chem.* **2012**, *22*, 1969.

(17) Lou, X. W.; Archer, L. A. *Adv. Mater.* **2008**, *20*, 1853.

(18) Lou, X. W.; Yuan, C.; Zhang, Q.; Archer, L. A. *Angew. Chem., Int. Ed.* **2006**, *45*, 3825.

(19) Liang, H. F.; Wang, Z. C. *Mater. Lett.* **2013**, *96*, 12.

(20) Murali, S.; Dreyer, D. R.; Valle-Vigón, P.; Stoller, M. D.; Zhu, Y.; Morales, C.; Fuertes, A. B.; Fuertes, C. W.; Ruoff, R. S. *Phys. Chem. Chem. Phys.* **2011**, *13*, 2652.

(21) Fang, B.; Kim, J. H.; Kim, M.-S; Bonakdargour, A.; Lam, A.; Wilkinson, D. P.; Yu, J.-S. *J. Mater. Chem.* **2012**, *22*, 19031.

(22) Chen, J. F.; Lang, Z. L.; Xu, Q.; Zhang, J. N.; Fu, J. W.; Chen, Z. M. *Phys. Chem. Chem. Phys.* **2013**, *15*, 17786.

(23) Chen, Y.; Chen, H. G.; Zeng, D. P.; Tian, Y. B.; Chen, F.; Feng, J. W.; Shi, J. L. *ACS Nano* **2010**, *4*, 6001.

(24) Ozaki, M.; Kratohvil, S.; Matijevic, E. *J. Colloid Interface Sci.* **1984**, *102*, 146.

(25) Ma, F. W.; Zhao, H.; Sun, L. P.; Li, Q.; Huo, L. H.; Tian, X.; Gao, S.; Pang, G. S.; Shi, Z.; Feng, S. H. *J. Mater. Chem.* **2012**, *22*, 13464.
(26) Liu, J.; Qiao, S. Z.; Liu, H.; Chen, J.; Orpe, A.; Zhao, D. Y.; Lu, G. Q. *Angew. Chem., Int. Ed.* **2011**, *50*, 5947.
(27) Zhang, J. N.; Guo, S. J.; Wei, J. Y.; Xu, Q.; Yan, W. F.; Fu, J. W.; Wang, S. P.; Cao, M. J.; Chen, Z. M. *Chem.—Eur. J.* **2013**, *19*, 16087.
(28) Guo, Y. J.; Guo, S. J.; Ren, J. T.; Zhai, Y. M.; Dong, S. J.; Wang, E. K. *ACS Nano* **2010**, *4*, 4001.
(29) Guo, S. J.; Wen, D.; Dong, S. J.; Wang, E. K. *ACS Nano* **2010**, *4*, 3959.
(30) Guo, Y.; Deng, L.; Li, J.; Guo, S. J.; Wang, E. K.; Dong, S. J. *ACS Nano* **2011**, *5*, 1282.
(31) Zhang, W.-M.; Wu, X.-L.; Hu, J.-S; Guo, Y.-G.; Wan, L.-J. *Adv. Funct. Mater.* **2008**, *18*, 3941.
(32) He, C. N.; Wu, S.; Zhao, N. Q.; Shi, C. S.; Liu, E. Z.; Li, J. J. *ACS Nano* **2013**, *7*, 4459.
(33) Yu, C.; Sun, Y. F.; Fan, X. M.; Zhao, Z. B.; Qiu, J. S. *Part. Part. Syst. Charact.* **2013**, *30*, 637.
(34) Couchman, P. R.; Jesser, W. A. *Nature* **1977**, *269*, 481.
(35) Zhang, J. N.; Ma, Z.; Jiao, J.; Yin, H. F.; Yan, W. F.; Hagaman, E. W.; Yu, J. H.; Dai, S. *Langmuir* **2009**, *25*, 12541.
(36) Zhang, J. N.; Ma, Z.; Jiao, J.; Yin, H. F.; Yan, W. F.; Hagaman, E. W.; Yu, J. H.; Dai, S. *Microporous Mesorporous Mater.* **2010**, *129*, 200.
(37) Chen, L.-F.; Zhang, X.-D.; Liang, H.-W.; Kong, M. G.; Guan, Q.-F.; Chen, P.; Wu, Z.-Y.; Yu, S.-H. *ACS Nano* **2012**, *6*, 7092.
(38) Jiang, S. J.; Ma, Y. W.; Jian, G. Q.; Tao, H. S.; Wang, X. Z.; Fan, Y. N.; Lu, Y. N.; Hu, Z.; Chen, Y. *Adv. Mater.* **2009**, *21*, 4953.
(39) Liu, X. H.; Zhou, L.; Zhao, Y. Q.; Bian, L.; Feng, X. T.; Pu, Q. S. *ACS Appl. Mater. Interfaces* **2013**, *5*, 10280.
(40) Wei, J. Y.; Zhang, J. N.; Liu, Y.; Xu, G. H.; Chen, Z. M.; Xu, Q. *RSC Adv.* **2013**, *3*, 3957.
(41) Sheng, K. X.; Sun, Y. Q.; Li, C.; Yuan, W. J.; Shi, G. Q. *Sci. Rep.* **2012**, *2*, 247.
(42) Wu, Q.; Xu, Y. X.; Yao, Z. Y.; Liu, A. R.; Shi, G. Q. *ACS Nano* **2010**, *4*, 1963.
(43) Wang, K. X.; Wang, Y. G.; Wang, Y. R.; Hosono, E.; Zhou, H. S. *J. Phys. Chem. C* **2009**, *113*, 1093.
(44) Li, W. R.; Chen, D. H.; Li, Z.; Shi, Y. F.; Wan, Y.; Wang, G.; Jiang, Z. Y.; Zhao, D. Y. *Carbon* **2007**, *45*, 1757.
(45) Kim, M.-S.; Fang, B. Z.; Kim, J. H.; Yang, D.; Kim, Y. K.; Baec, T.-S.; Yu, J.-S. *J. Mater. Chem.* **2011**, *21*, 19362.